Handling shape and contact location uncertainty in grasping two-dimensional planar objects

Vassilios N. Christopoulos and Paul Schrater

Abstract— **This paper addresses the problem of selecting contact locations for grasping objects in the presence of shape and contact location uncertainty. Focusing on two-dimensional planar objects and two finger grasps for simplicity, we present a principled approach for selecting contact points by analyzing the risk of force closure failure. The key contribution of this paper is the development of a method that incorporate shape uncertainty into grasp stability analysis. We propose a grasp quality metric that can be used to identify stable contact regions in the face of shape and contact location uncertainty. The proposed method successfully distinguishes grasps that are equivalent without uncertainty, and we illustrate the properties of this technique with simulation experiments in two classes of objects.**

I. INTRODUCTION

One of the most important problems in grasping and manipulation is the selection of contact points to grasp an object. Grasping involves fixuring the object relative to a gripper, and forms a necessary condition for object manipulation without changing object or finger contacts. Grasp planning requires a method of evaluating the potential quality of contact points for fixturing the object. Solutions to this problem involve specifying an appropriate grasp quality measure and an algorithm that optimizes this measure to formulate a reaching plan. A successful reaching plan directs the fingers to contacts on the object that are both high quality and achievable by the particular robotic gripper.

Consider the challenge posed by the following scenario: An agent equipped with a robotic arm and a camera operates in dynamic environments with the goal of grasping visually sensed but otherwise unknown objects. To select stable contacts, the agent must have access to the 3D geometry of the object. However, objects for which many surface locations are visually foreshortened or occluded in the image produce significant errors in 3D reconstruction. How to perform grasp analysis under these conditions is an open question. Because grasp quality will depend on errors in 3D reconstruction, the effects of shape uncertainty on grasp stability should be included in identifying stable contact locations. The main contribution of this paper is to show how to incorporate shape uncertainty into grasp stability analysis, and to provide a novel grasp quality metric that can be used to optimize contact selection in the face of shape uncertainty.

Vassilios N. Christopoulos is with the Computer Science and Engineering Department, University of Minnesota, 200 Union Street SE, Minneapolis, MN, USA vchristo@cs.umn.edu

Paul Schrater is with the Faculty of Computer Science and Engineering Department, University of Minnesota, 200 Union Street SE, Minneapolis, MN, USA schrater@umn.edu

Work on grasp measures have led to a variety of theoretical proposals that revolve around notions of force or form closure. These measures take as input a model of object contours (2D) or object surface (3D), the number and the type of contacts (point/soft, with/without friction), and return a quality score for each set of possible contacts [1].

In this type of analysis, grasp contact with an object of known geometry is modeled as N point (or line) contacts, that are one of several types: frictionless, frictional, or soft point. The wrenches that end-effectors can exert at these contacts vary with type. For example, frictionless permits only forces along the direction of the normal vector, while frictional also permits forces along the direction of the tangential vector [1].

Force (form) closure occurs when the sum of the set of wrenches (vectors containing forces and moments) at frictional (frictionless) contact points can equilibrate an external wrench. A set of contact locations are considered viable for force closure if any external wrench can be canceled by a suitable scaling of the contact wrenches, and the number of contacts required for viability under various conditions to achieve force (form) closure are known [2].

One of the simplest kinds of grasp quality score is a force (form) closure score, a binary number that indicates whether a grasp at a set of contacts is viable [3]. With perfect sensing and positioning, this measure does not distinguish between viable points–in the extreme, all contact locations may be viable for force closure (e.g. a sphere). Grasp quality metrics suffer from ambiguities of this kind, requiring planning algorithms to use other aspects of the grasp to select contact points (like reach path or wrench magnitude) from the viable set.

However, force closure ambiguity is largely eliminated by contact perturbations introduced by shape and finger location uncertainty. Ignoring the uncertainty that exists in real robotic systems will generate grasp failures for plans that appear viable. This paper proposes an approach for evaluating grasp quality in the presence of uncertainty. In particular, we show how to compute the probability of force-closure grasp, quantifying shape uncertainty using statistical shape analysis and introducing approach coordinates to handle variability in finger positioning and contact location.

This paper is organized as follows. Initially, we review the relative studies for identifying contact locations under variety of conditions including deterministic and uncertain cases. Thereafter, Section III presents a real world scenario where the geometry of an object is known imprecisely due to visual sensing. Sections IV and V demonstrate the necessary theory that is used to build the proposed technique for computing

Preprint submitted to 2007 IEEE/RSJ International Conference on Intelligent Robots and Systems. Received April 9, 2007.

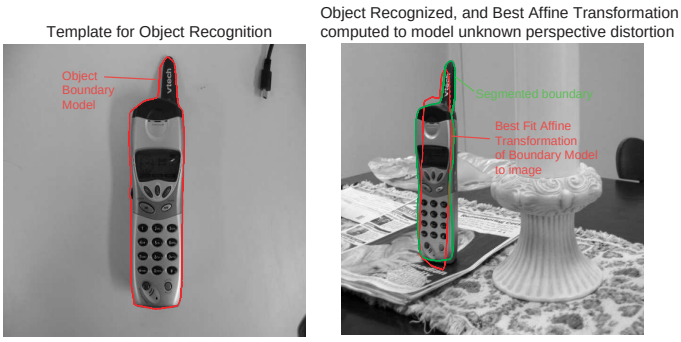

Fig. 1. Illustration of the origins of shape uncertainty. Template matching used to recognize and localize a target object in a scene, in this case a phone. **Left**: Target object is specified and segmentation is used to create a contour template. **Right**: Recognition and template transformation are determined using SIFT keypoints - a set of reliable feature points determined on the target object and found in the scene image. An affine transformation is estimated (poorly) between the feature point locations on the target object and their locations in the scene. This transformation forms a simple (paraperspective) model [4] of the image deformation under perspective projection. The affine transformation can be inverted to view the detected object from the front. However, the transformation has errors in it that creates uncertainty in the understanding of the detected shape.

stable contact locations under shape and contact locations uncertainty. Finally, Section VI presents the simulation results for grasping two classes of planar objects using the proposed technique.

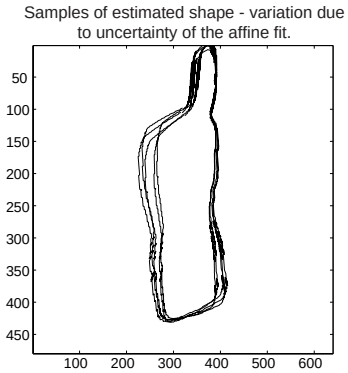

Fig. 2. Effect of matching errors on shape understanding. The error in shape understanding of the object in Fig. 1 right can be visualized by propagating Monte Carlo samples of the feature point matching error to the affine transformation estimates, generating a set of affine transformation samples. The affine matrices can be inverted and applied to the segmented object boundary in the scene, approximately inverting the perspective distortion. The result of this procedure is a set of possible object shapes. Given this sensing method it is not possible to know which of these samples represents the actual shape.

II. Related Work

In previous studies one of the principle ideas is to treat grasp selection as a constraint optimization problem [5]. Based on this approach, a number of objective functions are used for maximizing a grasp quality measure subject to various constraints, including: aspects of grasp task (e.g, exerted forces), object geometry (e.g., shape, dimension) and/or hand (gripper) characteristics (e.g., degrees of freedom). Grasp quality proposals include force (form) closure [2], resistance to slipping [6], [7], the number of degrees of freedom in object-hand linkage [8] (the number of independent parameters that are needed to specify the position and the orientation of the grasped object with respect to the hand), and grasp isotropy. All of these measures depend on the type of contacts and object geometry, and hence will be affected by changes in either contact or geometry. In addition, none of these measures are designed to handle uncertainty–they assume that the grasping environment is deterministic. Although it is widely appreciated that uncertainty adversely affects grasping, previous work involving grasp planning with different kinds of uncertainty is more limited.

A Bayesian approach for grasping an object with orientation uncertainty is presented in [9]. Assuming no information about initial object orientation, the goal of this approach is to move an object to a desired final state by a sequence of actions that minimize expected cost, where cost is measured in terms of the type and number of required actions. Another approach to grasp an object with orientation uncertainty is presented in [10]. This method is based on estimating the space of grasping motions (i.e., squeeze-grasp, offset-grasp and push-grasp), that guarantee stable grasp of two dimensional planar objects with unknown pose using a parallel-jaw gripper. However, neither of these studies consider shape and contact location uncertainty, and both use frictionless point contacts (form closure) constraints.

Several authors have looked at finger uncertainty in grasping. In [11], the finger uncertainty is analyzed using perturbation of object-finger locations with friction uncertainty. A new metric for measuring the sensitivity of grasp to contact uncertainty is presented in [12]. Approximating shape of a $2D$ planar object with a polygon, the goal of this work is to determine the maximum torque magnitude that the equilibrium grasp can resist. Based on this measure, the effect of positional error on the static equilibrium of the grasp can be determined.

Methods to make grasp plans robust to unknown object identity and friction errors introduced by visual sensing are presented in [13], [14], [15]. However, these methods do not model uncertainty nor do they consider its impact on grasp quality. We are aware of no previous work on the effects of shape uncertainty on grasp quality.

III. Shape Uncertainty due to Visual Sensing

Shape uncertainty occurs whenever object geometry is known imprecisely due to imperfect sensing (e.g., perspective projection). For example, consider estimating the shape of the cell phone in Fig. 1 using a model-based object segmentation algorithm and a pin-hole camera. The projected shape of the phone is geometrically distorted away from the model shape due to a different acquisition viewpoint [16]. However, there is an affine transformation that (approximately) relates the two shapes [17] (described below). The problem is that errors in the match between object and template can be

Preprint submitted to 2007 IEEE/RSJ International Conference on Intelligent Robots and Systems. Received April 9, 2007.

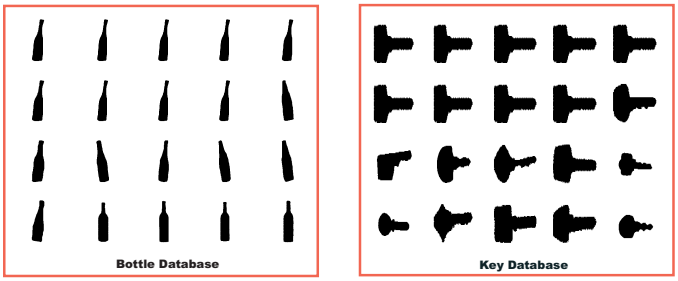

Fig. 3. Datasets with 20 bottles (left) and 20 keys (right) with shape variation used in this work for evaluating the proposed quality metric of grasping.

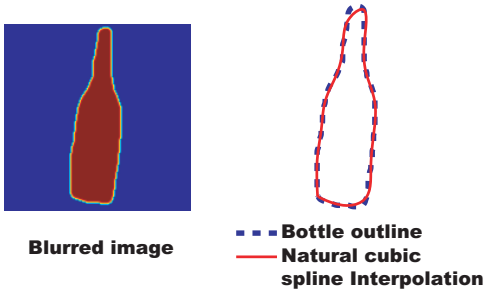

Fig. 4. **Left**: Blurred image using binomial filter. **Right**: Extracted boundary of a typical sample from the bottle database using model-based object segmentation technique (blue discontinuous line) and natural cubic spline interpolation (red continuous line).

absorbed into the affine transformation that encodes object pose.

For systems that use flexible templates [18], shape and pose are jointly estimated so that errors in both matching and pose generates uncertainty about the shape of phone [19]. For this case, the position of the camera with respect to the phone creates uncertainty about its geometric characteristics. Fig. 2 shows a set of possible phone shapes, which have been generated by taking images under different viewpoints and applying affine transformation. Clearly, following the aforementioned procedure, it is not possible to know which of the estimated shapes correspond to the actual shape of the phone. Hence, we need to maintain the uncertainty about the estimated shape of the objects during grasp planning.

IV. Methodology

In this section we provide the necessary background both on modeling shape statistically and on necessary conditions for force-closure grasp. This theory will be used to develop a method for computing the quality of grasp plans.

A. Data Preprocessing and object recognition

Assume that we have a set of two-dimensional planar objects resulting from image segmentation (e.g. bottles or keys) that belong to the same class but exhibit shape variation (or uncertainty), Fig. 3. Initially, we blur segmented images using binomial filters to remove small details and to smooth the outlines of the objects [20].

To extract curves from segmented images, we extract a chain of points on the object's boundary and construct an arc-length parameter from the cumulative distance between points. Finally, the N points are interpolated using smoothing "natural" cubic splines (illustrated in Fig. 4) which can be converted to B-spline form via a linear transformation.

B. Shape description using splines

We restrict our attention to spline curve and surface representations due to their simplicity and the ease of specifying shape uncertainty in spline models. We assume that any differences between the actual object surface and the spline representation do not affect significantly the results of contact analysis. This assumption is reasonable for soft-finger contacts with the object. For planar objects, a closed simply connected shape can be represented as a linear combination of B-splines defined on an arc-length parameter, Eq. (1).

$$\begin{aligned}[x(s)\,y(s)] &= \sum_{i=0}^{n} B^i(s) \begin{bmatrix} a_i^x \\ a_i^y \end{bmatrix} = \begin{bmatrix} \vec{B}(s)^T & \vec{0}^T \\ \vec{0}^T & \vec{B}(s)^T \end{bmatrix} \vec{a} \\ &= \mathbf{B}(s)\vec{a} \end{aligned} \tag{1}$$

where $B^i(s)$ are periodic cubic B-spline functions defined on a knot sequence on the arc-length parameter s, $[x(s)\,y(s)]$ are the cartesian (world coordinates) of the curve and $\vec{a} = \left[\vec{a_x}^T\ \vec{a_y}^T\right]^T$ is a $2nx1$ vector of coefficients that uniquely specify the shape given the knot sequence. It is straightforward to induce a probability distribution on shapes via $P(\vec{a})$. In general, this will be a density conditioned on the current image information.

The advantages of using a basis function representation for shape include low dimensional *shape-space* representations that are linear in transformation parameters. In addition, basis functions provide simple ways of computing important curve properties like tangents and normals. In particular, the unnormalized tangent at each point s' are linear in the shape parameters and is given by Eq. (2).

$$[t_x(s), t_y(s)] = \mathbf{D}(s')\vec{a} \tag{2}$$

where $\mathbf{D}(s) = d\mathbf{B}(s)/ds$. Given an counterclockwise parametrization of the curve, the unnormalized normal at each point s' is given by Eq. (3).

$$[n_x(s)\,n_y(s)] = \begin{bmatrix} 0 & -1 \\ 1 & 0 \end{bmatrix} \mathbf{D}(s')\vec{a} = \mathbf{N}(s')\vec{a} \tag{3}$$

As explained in the introduction, a common source of shape uncertainty is the distortion due to camera calibration and/or image matching errors. These errors produce affine distortions of the object contours [18]. For example, the projected shape of a $3D$ planar curve can be represented in shape-space through Eq. (4).

$$\vec{a} = \mathbf{W}\vec{q} \tag{4}$$

where $\mathbf{W}$ is given by Eq. (5)

$$\mathbf{W} = \begin{bmatrix} \mathbf{1} & \mathbf{0} & \vec{a}_0^x & \mathbf{0} & \mathbf{0} & \vec{a}_0^y & \vec{a}_0^z & \mathbf{0} \\ \mathbf{0} & \mathbf{1} & \mathbf{0} & \vec{a}_0^y & \vec{a}_0^x & \mathbf{0} & \mathbf{0} & \vec{a}_0^z \end{bmatrix} \tag{5}$$

and $\vec{a}_0^x$, $\vec{a}_0^y$, and $\vec{a}_0^z$ are the 3D coordinates of the base shape of the curve. In this representation, the components of $\vec{q}$ represent translation, scaling and rotation of the base curve in 3D, and $\mathbf{W}\vec{q}$ maps the effect of these changes on the projected contour. Note that a probability distribution on the reduced space $\vec{q}$, $P(\vec{q})$, induces distributions on the curve, tangents and normals through linear operators. We will take advantage of this in our formulation of the optimal grasping problem given shape uncertainty.

C. Finding grasp equilibrium

It is known that the force-closure grasp is necessary property for equilibrium [2]. Assume that we have two contact points A and B on the outline of an arbitrary object, Fig. 5 left.

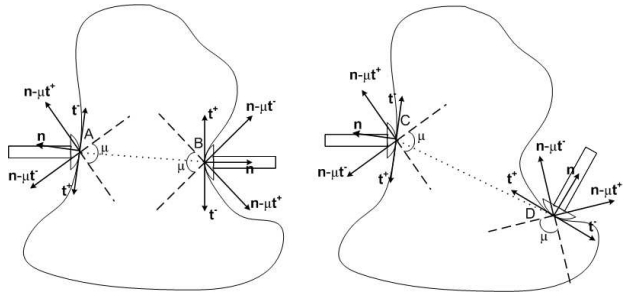

Fig. 5. **Left**: The contact points A and B construct a planar force-closure grasp, since the segment AB is between the two friction cones defined at the points A and B. **Right**: The contact points C and D do not construct force-closure grasp, because the segment CD is outside of the friction cone defined at the point D.

These points permit force-closure grasp, since the segment AB (or BA) is located inside the two friction cones that are defined by the contact points A and B. Using Coulomb's law, force closure occurs when the component of the contact forces at the points A and B in the direction of the surface normals ($\mathbf{n}$) exceeds the coefficient of friction times the tangential component . Geometrically, this relation produces friction cones, whose boundaries are determined by the vectors $\mathbf{n}-\mu\mathbf{t}^+$ and $\mathbf{n}-\mu\mathbf{t}^-$, where μ is the friction coefficient and $\mathbf{t}$ is the tangent vector, with $\mathbf{t}^+ = \mathbf{t}$ and $\mathbf{t}^- = -\mathbf{t}$.

Thus testing for force closure is equivalent to testing whether the segment AB is between the two friction cones. To illustrate, if the segment is out of one or both friction cones (e.g., Fig. 5 right), the two points do not construct a planar force closure and the object cannot be grasped from these two points. In other words, if we define $\mathbf{D_{AB}}$ as the vector from contact point A to B, these two points permit force closure, if the inequalities in Eqs. (6), (7), (8) and (9) hold.

$$(\mu\hat{\mathbf{n}}_A + \hat{\mathbf{t}}_A)\mathbf{D_{AB}} \leq \mathbf{0} \quad (6)$$

$$(\mu\hat{\mathbf{n}}_A - \hat{\mathbf{t}}_A)\mathbf{D_{AB}} \leq \mathbf{0} \quad (7)$$

$$(\mu\hat{\mathbf{n}}_B + \hat{\mathbf{t}}_B)(-\mathbf{D_{AB}}) \leq \mathbf{0} \quad (8)$$

$$(\mu\hat{\mathbf{n}}_B - \hat{\mathbf{t}}_B)(-\mathbf{D_{AB}}) \leq \mathbf{0} \quad (9)$$

V. Determining feasible locations in planar objects

Assume that a planar object can be represented by N contact points following the procedure that we have described in section IV-B. The ultimate goal is to find a feasible set of contact locations to provide an input to reach planning, using the Eqs. (6), (7), (8) and (9). However, object coordinates (even landmarks) are not stable from the hand's point-of-view in the presence of shape uncertainty and cannot be used directly for planning.

A. Approach space

To handle this problem, we compute the feasibility of a grasp plan, by computing the probability that a grasp plan will result in contact locations that form force-closure grasp of the object. To make this solution practical, we focus on the reaching movement near the object boundary (the *approach*), where we assume finger trajectories can be approximated by line segments. Thus for two-finger planar grasps, the approach space requires 3 parameters per finger, to specify the origins and directions of the line segments, Eq. (10).

$$\vec{l}_i(\lambda) = \vec{x}_{0,i} + \lambda\,[\cos(\theta_i)\sin(\theta_i)] = \vec{x}_{0,i} + \lambda\vec{u}(\theta_i) \quad (10)$$

where $\theta_i\ \varepsilon\,[0, 2\pi]$ is the direction of the finger i for grasping the object, $\vec{x}_{0,i}$ corresponds to the origin of the finger i, and λ is the scale variable of the line segment. In this case, grasp plans with equivalent approaches are represented as points $\vec{g} = \{\vec{x}_{0,1}, \vec{x}_{0,2}, \theta_1, \theta_2\}$ in an approach space $(\Re^4, S^2)$. For every approach under consideration, we need to compute the probability of successful force-closure grasp. To simplify our analysis, we focus on grasp plans in which the finger's line segments intersect somewhere inside the boundary of the object, $\vec{x}_0$, which is called the "approach center". Given an approach, we can compute the possible contact locations of an object with shape uncertainty without using world coordinates. In this way, the choice of approach can be made without exact determination of the contact location on the actual object.

Fig. 6 shows an example of three objects that belong to the uncertainty set. Based on the approach, we can compute the contact point locations (red dots) for any value of the uncertain shape parameters $\vec{q}$.

Although the analysis is more complicated for extended fingers and non-linear paths, approach analysis can be performed in these cases as well.

B. Feasibility analysis of planar objects with shape uncertainty

We decompose into two parts the problem of computing the probability of force-closure grasp. One part of the analysis is to compute the probability across contact locations given a set of approach coordinates. The probability across contact points incorporates both shape uncertainty and noisy execution of the reach. The second part focuses on computing the probability that a grasp will result in force closure for each set of contact locations.

Preprint submitted to 2007 IEEE/RSJ International Conference
on Intelligent Robots and Systems. Received April 9, 2007.

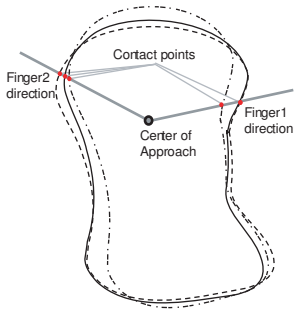

Fig. 6. Computing contact locations in the approach space. Assuming that the direction of the fingers are intersected in the center of approach, the contacts (red dots) depend on the fingers' angular position and not on the shape's coordinates.

For any pair of contact points $\{\vec{x}_{c1},\vec{x}_{c2}\} = \{\mathbf{B}(s_1^*)W\vec{q},\mathbf{B}(s_2^*)W\vec{q}\}$ that result from following an approach $\vec{g}_e$, we define a feasibility indicator function $f = \mathbf{I}(\vec{q},\vec{x}_{c1},\vec{x}_{c2})$, where $\vec{q} = [q_1,q_2,\dots q_m]$ describes the parameters of the object outline. The indicator function returns 1 if the Eqs. (6), (7), (8) and (9) hold and 0 otherwise. Using this indicator function, the probability that an executed approach is feasible is given by Eq. (11)

$$P(f=1|\vec{g}_e) = \int_{q_1}\int_{q_2}\dots\int_{q_n} \mathbf{I}(\vec{q},\vec{x}_{c1},\vec{x}_{c2})P(\vec{q})d\vec{q} \qquad (11)$$

For any particular shape, the contact points can be found from the executed approach, $\overrightarrow{g_e}$, by finding the intersection of the finger's line segment paths with the shape. The computation of the first intersection with the control polygon of the shape's spline curve is simple. We refine this intersection to lie on the spline curve numerically (for 4^{th} order or less B-spline curves, the points can be found by solving the intersection of a line segment and polynomial), resulting in locations on the curve $s_1^*(\vec{g}_e,\vec{q}), s_2^*(\vec{g}_e,\vec{q})$. The force closure conditions are then straightforward to write explicitly in terms of the shape parameters. For instance, using Eqs. (2), (3) and (4), we can rewrite Eq. (6) as follows:

$$\begin{aligned}\gamma_1 = (\mu\mathbf{N}(s_1^*)\vec{a} - \mathbf{D}(s_1^*)\vec{a})^T(\mathbf{B}(s_2^*)\vec{a} - \mathbf{B}(s_1^*)\vec{a}) &< 0 \Rightarrow \\ ((\mu\mathbf{N}(s_1^*) - \mathbf{D}(s_1^*))W\vec{q})^T(\mathbf{B}(s_2^*) - \mathbf{B}(s_1^*))W\vec{q} &< 0 \quad (12)\end{aligned}$$

In the same way, γ_2, γ_3 and γ_4 can be obtained from Eqs. (7), (8) and (9), respectively, using the terms of the shape parameters. If these inequalities hold, the executed approaches, $\vec{g}_e$, concludes to force-closure grasp. Overall, an indicator function that returns 1 when all four inequalities are satisfied can be similarly computed for every $(\vec{g}_e,\vec{q})$ pair. The pseudo-code of the aforementioned procedure for detecting contact locations that give force-closure grasp is presented in Fig. 7. $H(\cdot)$ describes the Heaviside step function, which in discrete form is given by Eq. (13).

$$H(n) = \begin{cases} 0, & n<0 \\ 1, & n\geq 0 \end{cases} \qquad (13)$$

For j = 1 to M sample approaches
  For i = 1 to N sample shapes
    sample shape:
    $P(\vec{a}) \rightarrow \vec{a}_{ij}$
    intersect object:
    $s_1^* \leftarrow$ intersect $(\vec{x}_{0,1},\ \theta_1,\ \vec{a}_{ij}\ )$
    $s_2^* \leftarrow$ intersect $(\vec{x}_{0,2},\ \theta_2,\ \vec{a}_{ij}\ )$
      compute force closure condition:
      $\gamma_1^{ij}(s_1^*,s_2^*) < 0$
      $\gamma_2^{ij}(s_1^*,s_2^*) < 0$
      $\gamma_3^{ij}(s_1^*,s_2^*) < 0$
      $\gamma_4^{ij}(s_1^*,s_2^*) < 0$
  end sample shape
    compute quality metric
    $\mathbf{Q}_j = \sum_{j=1}^{Nsamples} H(\gamma_1^{ij})H(\gamma_2^{ij})H(\gamma_3^{ij})H(\gamma_4^{ij})\ P(\vec{a}_{ij})$
end approach

Fig. 7. Pseudo-code of the procedure for identifying stable contact locations under shape uncertainty. The superscripts and subscripts i, j help convey that the stability measure and shape parameters vary within both loops. The H(.) corresponds to the Heaviside step function

Finally, we also want to include the effects of noisy execution of an approach by defining a conditional distribution of the executed approach, $\vec{g}_e$, given the desirable approach, $\vec{g}_{plan}$, $P(\vec{g}_e|\vec{g}_{plan})$. These effects should be taken into account in order to reduce the probability of grasp failure by reducing the feasibility of approaches that are sensitive to perturbations. The effect of noisy execution on the feasibility of $\vec{g}_{plan}$ is given by:

$$P(f=1|\vec{g}_{plan}) = \int_{\vec{g}_e} P(f=1|\vec{g}_e)P(\vec{g}_e|\vec{g}_{plan})d\vec{g}_e \qquad (14)$$

For small amounts of noise, the effects of noisy execution $P(\vec{g}_e|\vec{g}_{plan})$ can be approximated as Gaussian.

C. Computing probability of grasp stability via sampling

Contact locations can be selected by optimizing the grasp stability given by Eq. (14). However, straightforward optimization of the grasp stability measure is difficult due to the integrals in Eqs. (11) and (14). For this reason, we have used Monte Carlo integration. Sampling shapes from $P(\vec{q})$ and plans from $P(\vec{g}_e|\vec{g}_{plan})$, we compute the feasibility of each sample pair and average. In this work we focus on two special cases of approaches. First, the object is approached having both fingers intersect at a common point, $\vec{x}_0$ (i.e., approach center), inside the object's boundary. The fingers are assumed to be moved by actuators with independent noise. The desirable approach, $\vec{g}_{plan}$, is described by the $\{\phi_\alpha^*,\phi_\delta^*,\vec{x}_0\}$, where ϕ_α^*, ϕ_δ^* denote the desirable movement direction of the first and second finger, respectively. Let ϕ_α, ϕ_δ denotes the actual finger's movement direction near the object boundary, then for each approach center $\vec{x}_0$ the probability distribution for any grasp plan is given by Eq. (15),

$$P\left(\vec{g}_e|\vec{g}_{plan}\right) = P\left(\phi_\alpha|\phi_\alpha^*,\vec{x}_0\right)P\left(\phi_\delta|\phi_\delta^*,\vec{x}_0\right) \qquad (15)$$

A second important case is when the two fingers motions are constrained, as in a two finger parallel gripper where the fingers always move parallel to each other in opposite directions driven by a single actuator. In this case the probability distribution of grasp plans has the form in Eq. (16).

$$P\left(\vec{g}_e|\vec{g}_{plan}\right) \quad = \quad \delta(\phi_\delta - (\phi_\alpha + \pi))P(\phi_\alpha|\phi_\alpha^*, \vec{x}_0) \quad (16)$$

where $\delta(\cdot)$ is the dirac function that enforces the constraint that the approach directions of the two fingers oppose each other.

VI. Simulation Results

In this section, we illustrate and discuss the properties of grasp stability under uncertainty using two different object datasets from the Brown vision laboratory [21]. Each dataset contains 20 two-dimensional planar objects that belong to the same class but exhibit significant shape variation. The shape variation in this case is similar to the shape variation of objects due to the visual sensing that we discussed in Section III. To model noise in the approach execution, we assume a zero mean Gaussian distribution for Eq. (15) with variance 0.05 rad, whereas the friction coefficient is 1 (for simplicity and it is in the range of typical values of soft finger contact).

A. Determine feasible locations in the bottle database

Two different ways for approaching a typical sample from the bottle database is shown in Fig. 8. Although a standard force closure analysis does not distinguish them, case *I* is more desirable than case *II* in the presence of shape and contact location uncertainty, since there are more ways to generate feasible contact points. Thus, the probability measure is analogous to a motion perturbation analysis [11], since plans with the highest probability of feasibility are those that survive perturbations in finger locations. However, the strong point of the proposed method is that it handles not only perturbations in finger locations but also shape perturbations.

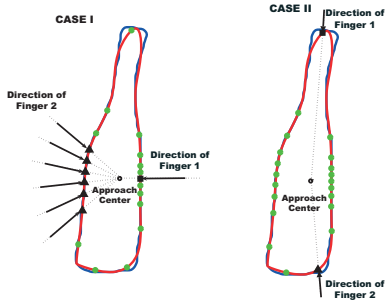

Fig. 8. Two different ways for reaching a typical sample from the bottle database. Selecting the "square" point as a location for the first finger, "triangles" points correspond to the candidate locations for the second finger, so that to construct force-closure grasp. The number of pairs of points that give force-closure grasp is larger in **case I** than **case II** and as a result the first case is considered more reliable (i.e., more stable) than the second one. The green points correspond to the possible contacts based on the approach.

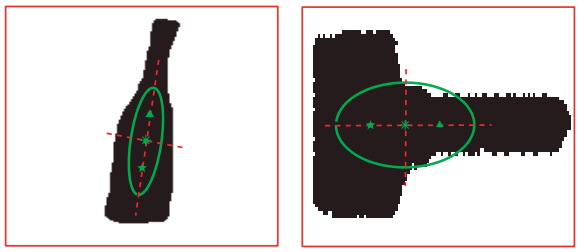

Fig. 9. Center of approach parameterized by the second moment of the objects' mass distribution. The second moment is represented by the ellipse, whereas the two dashed lines correspond to the major and minor axis of the ellipse. The center of mass (star) is the origin of the ellipse and we compute two points (triangle and pentagram) that lie on the major axis $\pm\sqrt{\lambda_1}/2$ from the center of mass, where λ_1 is the principal eigenvalue. The **left** and the **right** figures show the second moment of a typical sample from the bottle and the key database, respectively.

The results of estimating Eq. (14) by sampling both approach directions and boundaries of bottles are shown in Fig. 10. To help visualize the results, the center of approach is fixed at several locations, chosen along the long axis of the second moment of the boundary points (see Fig. 9), centered around the center of mass of the bottle dataset. The probability of a feasible grasp is displayed as a function of the first and second finger approach directions. The intersection of a set of finger directions with a typical sample of a bottle boundary is displayed next to the probability maps, sampled at 0.3 rad (i.e., $2\pi/0.3 \approx 21$ contact points).

The red areas correspond to pairs of finger directions with high probability to produce force-closure grasp. In contrary, blue areas correspond to unreliable regions for grasping the bottles, since the probability to obtain force-closure grasp is very low. Hence, the probability to achieve a stable grasp is higher (i.e., red regions) grasping the bottle around its "body" than grasping it from up to down (i.e., blue "islands"). It should be pointed out that almost all regions would permit force-closure grasp in an analysis ignoring shape and contact location uncertainty. However, the proposed quality metric of grasping shows that some regions are more reliable for grasping the bottle than others. It should be pointed out that the symmetry in the probability is due to a presumption of exchangeability of finger 1 and 2.

The effect of varying the approach center is shown in Figs. 10(a), 10(b) and 10(c). Note that the approach center has very little impact on feasibility, since the feasible regions for grasping the bottles are almost the same for the three cases. In other words, there are many points that are equally good for grasping elongated objects like the bottles.

B. Determine feasible locations in the key database

In addition to the bottle dataset, we compute the probability distribution of feasible regions for a database of keys, Fig. 3 right. The keys were chosen because under increasing blur they converge to shapes similar to bottles. Moreover, Fig. 13 shows that the good and bad approach directions for the keys should be similar to the bottles, once the object's main axes are matched. Nevertheless, we show that these two

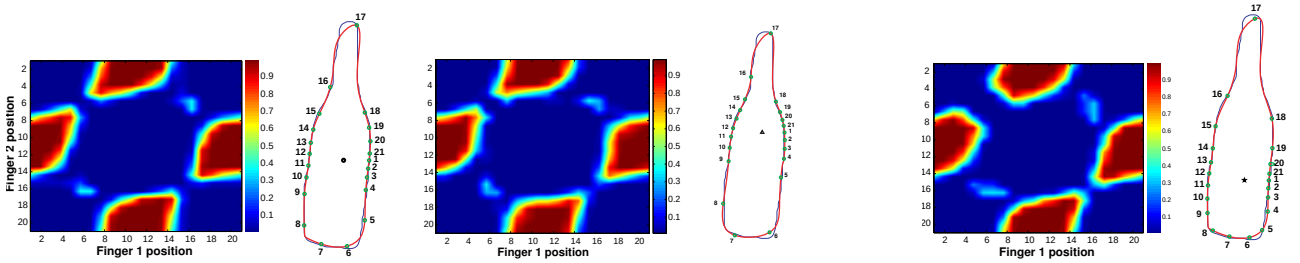

(a) Grasp plan I: Center of mass (b) Grasp plan II: $\sqrt{\lambda_1}/2$ from the center of mass (c) Grasp plan III:-$\sqrt{\lambda_1}/2$ from the center of mass

Fig. 10. Probability distribution of the feasible regions for three different approach centers (see Fig. 9). Note that the pattern of feasible regions is almost independent from the approach center.

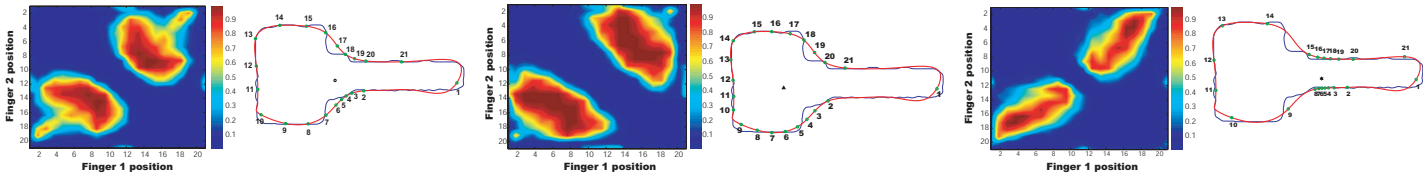

(a) Grasp plan I: Center of mass (b) Grasp plan II: $\sqrt{\lambda_1}/2$ from the center of mass (c) Grasp plan III:-$\sqrt{\lambda_1}/2$ from the center of mass

Fig. 11. Probability distribution of the feasible regions for three different approach centers (see Fig. 9). In contrast to the case of bottle, the approach center affects the distribution of feasible regions for the key case.

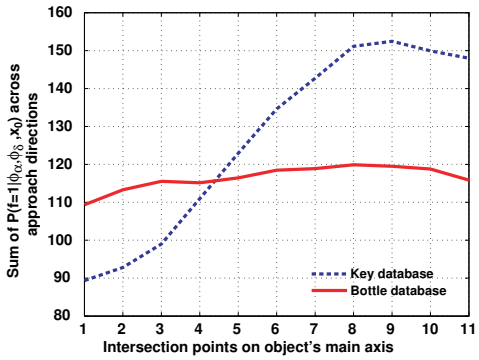

Fig. 12. Integration of the probability maps across finger approach directions for 11 different approach centers along the main axis of the objects.

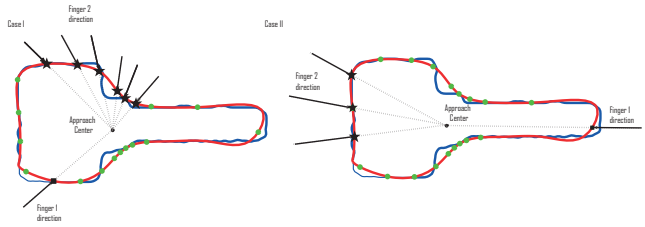

Fig. 13. Two different ways for reaching a typical sample from the key database. Selecting the "square" point as a location for the first finger, the "star" points correspond to the candidate contact points for second finger, so that the pair of contacts to construct force-closure grasp. The number of pairs that produce force-closure grasp is larger in **case I** than **case II** and as a result the first case is considered more reliable than the second one. The green points correspond to the possible contacts based on the approach directions.

classes of objects have different stability properties under uncertainty.

Performing an analysis identical to the bottle case, the probability distribution of the feasible regions for different approach centers are shown in Figs. 11(a), 11(b) and 11(c). Note that the most "reliable" regions are around the "head" of the key. Furthermore, moving the approach center from the "head" to the "teeth" part of the key the probability of producing a force-closure grasp decreases. Thus, in contrast to the bottle case, the planned approach center matters for the case of key.

C. *Effects of approach center and finger coupling on stability*

The simulation results show that the approach center of grasping an object may significantly affect the probability distribution of the feasible regions. To quantify this effect, we integrated the probability maps across finger approach directions for 11 different approach centers (± 0.2 of the leading eigenvalue) along the object's main axis (principal eigenvector), for both bottles and keys. This provides a simple measure of the number of approaches that permit force-closure grasp for a given approach center. The results are shown in Fig. 12. While the curve is essentially flat for the bottle database, approaching the key around its "head" significantly improves the chances of achieving force closure.

Preprint submitted to 2007 IEEE/RSJ International Conference on Intelligent Robots and Systems. Received April 9, 2007.

Finally, we investigate the effect of finger coupling that results from a parallel two jaws gripper. In this case, the angular positions of the two fingers are dependent and their directions are opposite. The probability distribution of the feasible regions is shown for both bottle and key database in Fig. 14.

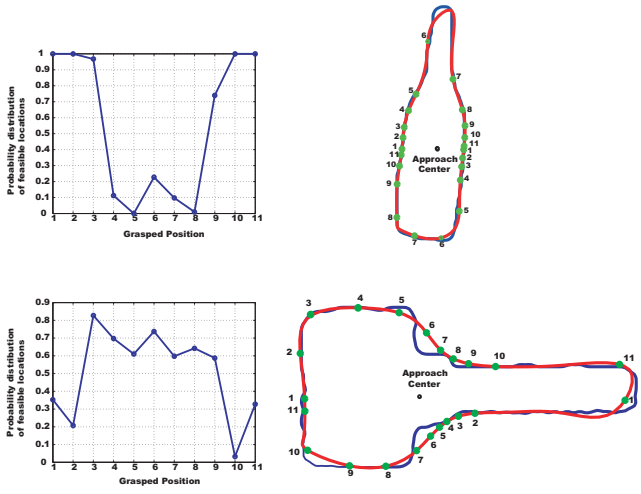

Fig. 14. Probability distribution of the feasible regions using parallel two jaws gripper. Clearly, only the pairs of contact locations (i,i), with $i = 1, \ldots, 11$ (green points) can be grasped by the parallel two jaws gripper.

The intersection of a set of finger directions with a typical sample of the object boundary is displayed next to the probability distribution maps, sampled at $0:2856$ rad (i.e., $\approx$ 22 contacts). Similar to the previous results, the probability to obtain force-closure grasp is high when the contacts are around the "body" of the bottle, whereas it goes to zero grasping the bottles from up to down. Regarding the key database, note that there is not any grasp plan that gives force closure with probability 1. Finally, the advantage of grasping keys at the "head" emerges with the parallel gripper as well, which we believe accords well with intuition and practice for human grasping of individual keys.

VII. Conclusion

This paper presents a new approach to identifying stable regions for grasping objects in the presence of shape and finger contacts uncertainty. We have focused in two-dimensional planar objects approximating their shapes with B-spline functions. Modeling the contacts as frictional points, our goal is to compute the probability that a two-fingered grasp plan will result in a force-closure grasp of the object. The main contribution of this work is the development of a method that incorporates uncertainty into grasp stability analysis. We propose a novel quality metric that can be used to identifying stable contact regions taking into account both the object's shape and the finger placement uncertainty. This measure distinguishes the contact stability of points that are equivalent in a standard analysis without resorting to rolling contact or motion perturbations.

In a future work, we are planning to extend the proposed analysis for identifying stable contact locations to grasp 3 dimensional objects in the presence of shape and contact location uncertainty. In addition, we have designed and built a number of objects with specific geometric shapes (e.g., trapezoids, triangles) and we are planning to apply the proposed contact metric for grasping these objects using a robotic arm equipped with a camera.

VIII. Acknowledgments

This work is partially supported by NIH grant R01EY01526.

References

[1] A. Bicchi and V. Kumar, "Robotic Grasping and Contact: A Review," in *Proceedings of the IEEE International Conference on Robotics and Automation*, vol. 1, San Francisco, CA, Apr. 2000, pp. 348–353.

[2] V. D. Nguyen, "Constructing Force-Closure Grasps," *The International Journal of Robotics Research*, vol. 7, no. 3, pp. 3–16, Jun. 1988.

[3] A. M. Okamura, N. Smady, and M. R. Cutkosky, "A Overview of Dexterous Manipulation," in *Proceedings of the IEEE International Conference on Robotics and Automation*, vol. 1, San Francisco, CA, Apr. 2000, pp. 255–262.

[4] J. Aloimonos, "Perspective approximations," *J. Image and Vision Computing*, vol. 8, pp. 179–192, Aug. 1990.

[5] S. T. Venkataraman and T. Iberall, *Dextrous Robot Hands*. Springer-Verlag, 1990.

[6] J. R. Kerr and B. Roth, "Analysis of Multifingered Hands," *International Journal of Robotics Research*, vol. 4, no. 4, pp. 3–17, 1986.

[7] M. Cutkosky, "On Grasp Choice, Grasp Models, and the Design of Hands Formanufacturing Tasks," *IEEE Transactions on Robotics and Automation*, vol. 5, pp. 269–279, Jun. 1989.

[8] M. T. Mason and J. K. Salisbury, *Robot Hands and the Mechanics of Manipulation*. MIT press, May 1985.

[9] K. Y. Goldberg and M. T. Mason, "Bayesian Grasping," in *Proceedings of the IEEE International Conference on Robotics and Automation*, vol. 2, Cincinnati, OH, May 1990, pp. 1264–1269.

[10] R. C. Brost, "Planning Robot Grasping Motions in the Presence of Uncertainty," The Robotic Institute, Carnegie-Mellon, Pittsburgh, PA, Tech. Rep. CMU-RI-TR-85-12, Jul. 1985.

[11] Y. Zheng and W.-H. Qian, "Coping with the Grasping Uncertainties in Force-closure Analysis," *The International Journal of Robotics Research*, vol. 24, no. 4, pp. 311–327, 2005.

[12] G. M. Bone and Y. Du, "Multi-Metric Comparison of Optimal 2d Grasp Planning Algorithms," in *Proceedings of the IEEE International Conference on Robotics and Automation*, vol. 3, Seoul, Korea, May 2001, pp. 3061–3066.

[13] A. Blake, "Computational Modelling of Hand-Eye Coordination," *Philosophical Transactions: Biological Sciences*, vol. 337, no. 1281, pp. 351–360, 1992.

[14] J. A. Coelho and R. A. Grupen, "A Control Basis for Learning Multifingered Grasps," *Jounal of Robotic Systems*, vol. 14, pp. 545–557, Jul. 1997.

[15] A. D. P. A. Morales, P.J Sanz, "Vision-Based Computation of Three-Finger Grasps on Unknown Planar Objects," in *Proceedings of the IEEE Intelligent Robots and System*, vol. 2, Washington, DC, May 2002, pp. 1711–1716.

[16] B. K. P. Horn, *Robot Vision*, 1st ed. The Mit Press, 1986.

[17] S. Ullman and R. Basri, "Recognition by linear combinations of models." *IEEE Trans. on Pattern Analysis and Machine Intelligence*, vol. 13, no. 10, pp. 992–1006, 1991.

[18] A. Blake and M. isard, *Active Contours*, 1st ed. Springer-Verlag, 1998.

[19] G.Bebis, M.Georgiopoulos, N. Lobo, and M. Shah, "Learing Affine Transformations," *Pattern Recognition*, vol. 32, no. 10, pp. 1799–1999, Oct. 1999.

[20] R. C. Gonzalez and R. E. Woods, *Digital Image Processing*, 2nd ed. Pearson Education, 2002.

[21] Laboratory for Engineering Man/ Machine Systems, "2d planar database, http://www.lems.brown.edu/vision."